

Wavelength de-multiplexing properties of a single aperture flanked by periodic arrays of indentations

J. Bravo-Abad,¹ F.J. García-Vidal,¹ and L. Martín-Moreno²

¹*Departamento de Física Teórica de la Materia Condensada, Universidad Autónoma de Madrid, E-28049 Madrid, Spain*

²*Departamento de Física de la Materia Condensada, ICMA-CSIC, Universidad de Zaragoza, E-50009 Zaragoza, Spain*

In this paper we explore the transmission properties of single subwavelength apertures perforated in thin metallic films flanked by asymmetric configurations of periodic arrays of indentations. It is shown how the corrugation in the input side can be used to transmit selectively only two different wavelengths. Also, by tuning the geometrical parameters defining the corrugation of the output side, these two chosen wavelengths can emerge from the structure as two very narrow beams propagating at well-defined directions. This new ability of structured metals can be used as a base to build micron-sized wavelength de-multiplexers.

PACS numbers: 78.66.Bz, 73.20.Mf, 42.79.Dj, 71.36.+c

I. INTRODUCTION

The new technological abilities for structuring metals in the micro and nanometer length scales are triggering a renewed interest in the optical properties of metals^{1,2,3,4,5,6,7}. A breakthrough in the field was the experimental discovery⁸ that the optical transmission through an array of sub-wavelength holes is, for certain wavelengths, boosted orders of magnitude over what a theory of independent holes would predict.

In subsequent works it was shown how the transmission through a **single** aperture can be boosted if it is appropriately flanked by surface corrugations in the side light is impinging on^{9,10,11}. Corrugations on the exit surface practically do not modify the *total* transmittance but, for some resonant wavelengths, greatly modify the angular distribution of the transmitted light, leading to strong beaming effects^{11,12}. This was shown for a hole surrounded by corrugations in the so-called bull's eye geometry and for a single slit flanked by one-dimensional grooves. It has been shown that these two processes (enhanced transmission and beaming) work independently^{12,13}, so it is possible to have more light passing through an aperture and have it transmitted in a narrow beam by patterning both the input and exit sides. These effects are associated to the formation of electromagnetic resonances (leaky modes) running along the metal surface, and radiating as they move due to the coupling to homogeneous waves in vacuum. The spectral position of these EM resonances depend on the geometrical parameters defining the corrugations (distance between indentations, and their widths and depths).

These studies were done in a symmetric configuration of a finite number of grooves surrounding the central slit. In this paper we show that, to a large extent, the properties of the groove arrays at the left and right of the slit behave independently. This property adds to the interpretation of the properties of the system in terms of running surface waves. It also allows, through the appropriate choice of geometrical parameters for left and right groove arrays at both entrance and exit surfaces, this

type of structures to act as wavelength de-multiplexers: the input side of the device can be used as a filter for two particular wavelengths and the corrugations on the exit side can be tailored in order to beam each of these two chosen wavelengths in different directions.

The paper is organized as follows: in Section 2 we present the theoretical formalism. Section 3 presents the transmission results for a single slit with an array of groove to one side, while the transmission angular distribution is considered in Section 4. In Section 5, we show how this kind of structures may be used for wavelength demultiplexing (WDM).

II. THEORETICAL FORMALISM

We are interested in analyzing the transmission properties of the system depicted in Fig.1: a single slit flanked by finite arrays of one-dimensional rectangular indentations. The central slit may be flanked by arrays of grooves at both input and output metal surfaces and, in each case, the arrays may be different to the left and right of the slit. We refer to these four arrays as IL, IR, OL and OR (see Fig.1), depending on whether they are input-left, input-right, output-left and output-right, respectively. Each groove (α) is characterized by its position (r_α), its width (a_α) and its depth (h_α), while the slit (labelled by the sub-index 0) is considered to be placed at the origin, having a width a_0 . Metal thickness is W .

Let us concentrate in the case of p-polarized light for which interesting resonant effects have been reported. Electromagnetic (EM) fields associated to this scattering process are expanded by a set of plane waves in vacuum and by a modal expansion inside the indentations (slit and grooves). For this last case, as we are mainly interested in sub-wavelength apertures, we consider that only the fundamental propagating eigenmode is excited. Then, for x inside indentation α , the wavefield is a linear combination of $\phi_\alpha(x) \exp(\pm ikz)$, where $k = 2\pi/\lambda$ and $\phi_\alpha(x) = 1/\sqrt{a_\alpha}$. We assume that the metal behaves as a perfect metal, expelling the electric field from its

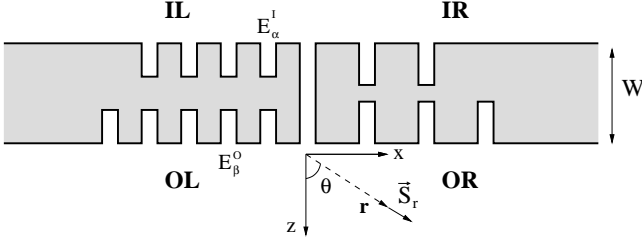


FIG. 1: Schematic illustration of the structure under study. IL, IR, OL and OR label the input-left, input-right, output-left and output-right arrays of grooves, respectively. The reference system considered is also plotted.

bulk. One advantage of the perfect metal approximation is that as all length scales associated to the dielectric constant (skin depth and absorption length) disappear from the problem, all results are directly exportable to other frequency regimes (microwave or infrared regimes), simply by scaling appropriately the geometrical parameters defining the structure. With respect to the applicability of this approach in the optical regime, we have demonstrated in previous theoretical works¹⁴ that this is a reasonable approximation when analyzing optical properties of nanostructured metals like silver or gold in simpler systems like reflection gratings or 1D arrays of subwavelength slits. Moreover, within this framework, we have been able to reproduce^{12,13} in semi-quantitative terms the reported phenomena of enhanced transmission and beaming appearing in the optical regime for finite structures.

In order to extract the expansion coefficients in vacuum (related to the reflection and transmission functions) and indentations regions, we match the parallel components of the EM fields (E_x and H_y) at the interfaces present in the system. By projecting the matching equation for E_x at $z = -W$ and $z = 0$ onto plane waves, we can express the reflection and transmission coefficients in terms of the wavefield expansion coefficients inside the indentations. H_y must be continuous only at the indentation openings and also (as we are assuming perfect metal boundary conditions) $E_x = 0$ at the bottom of the grooves. Therefore, all matching equations can be expressed as a function of the set of expansion coefficients inside the indentations: $[E_\alpha^I, E_\beta^O]$ (see Fig.1). The sub-set (E_α^I) give the x -component of the electric field at $z = -W^+$ through the equation: $E_x(x, z = -W^+) = \sum_\alpha E_\alpha^I \phi_\alpha(x)$, where α runs from $-N_L^I$ to $+N_R^I$ (N_L^I and N_R^I are the number of grooves to the left and right of the slit in the input side, respectively). (E_β^O) is related to the x -component of the electric field at the exit interface $z = 0^-$: $E_x(x, z = 0^-) = \sum_\beta E_\beta^O \phi_\beta(x)$, β running from $-N_L^O$ to $+N_R^O$ (N_L^O and N_R^O are the number of grooves to the left and right of the slit in the output side, respectively). In both expansions, sub-index 0 stems for the

central slit. After some elementary algebra, it is possible to find the set of $(N_L^I + N_R^I + N_L^O + N_R^O + 2)$ equations that govern the behavior of $[E_\alpha^I, E_\beta^O]$:

$$\begin{aligned} [G_{\alpha\alpha} - \epsilon_\alpha] E_\alpha^I + \sum_{\gamma \neq \alpha} G_{\alpha\gamma} E_\gamma^I - G_v E_0^O \delta_{\alpha 0} &= I_\alpha \quad (1) \\ [G_{\beta\beta} - \epsilon_\beta] E_\beta^O + \sum_{\eta \neq \beta} G_{\beta\eta} E_\eta^O - G_v E_0^I \delta_{\beta 0} &= 0 \end{aligned}$$

The first set of equations accounts for the expansion coefficients at the input interface and the sub-indexes α and γ run from $-N_L^I$ to N_R^I . Due to the normalization we use for the transmittance (see below), the illumination term I_α is equal to 2 for all α . The second set of equations is homogeneous (the output interface is not directly illuminated), and β and η ranges from $-N_L^O$ to N_R^O . Note that the only connection between the two interfaces is via the central slit and appears through the term $G_v E_0^O \delta_{\alpha 0}$ in the first set and by $G_v E_0^I \delta_{\beta 0}$ in the second one. In Refs.^{12,13} we explain in detail the origin and values of the different terms appearing in Eq.(1). For instance, $G_{\alpha\beta}$ is the contribution to the E_x field at indentation α coming from light scattered at indentation β . In fact, $G_{\alpha\beta}$ is the projection onto wavefields ϕ_α and ϕ_β ($G_{\alpha\beta} = \langle \phi_\alpha | G | \phi_\beta \rangle$) of the Green's function: $G(\mathbf{r}, \mathbf{r}') = \frac{i\pi}{\lambda} H_0^{(1)}(k | \mathbf{r} - \mathbf{r}' |)$, $H_0^{(1)}$ being the Hankel function of the first kind. $G_{\alpha\alpha} = \langle \phi_\alpha | G | \phi_\alpha \rangle$ is a self-interaction that takes into account the coupling of the eigenmode at indentation α with the radiative modes in vacuum regions. This quantity depends only on the ratio between indentation width and wavelength of light, a_α/λ . As said before, in this type of structures both sides of the corrugated metal film are only coupled by the term G_v that is a function of metal thickness: $G_v = 1/\sin(kW)$. The diagonal terms ϵ_α are related to the back and forth bouncing of the EM-fields inside indentation α : $\epsilon_\alpha = \cot(kh_\alpha)$ for $\alpha \neq 0$ and $\epsilon_0 = \cot(kW)$ for the central slit. Once the values for $[E_\alpha^I, E_\beta^O]$ are calculated, the total transmittance is a function of the amplitudes of the E-field at the entrance and exit of the central slit: $T = \text{Im} \{ E_0^I E_0^{O*} \} / \sin(kW)$.

Also the EM fields in real space can be expressed in terms of the set $[E_\alpha^I, E_\beta^O]$. For example, in the transmission region ($z > 0$):

$$H_y(\vec{r}) = \frac{1}{\mu_0 c} \sum_\alpha E_\alpha^O G(\alpha, \vec{r}) \quad (2)$$

all other components of the EM field can be obtained from $H_y(\vec{r})$ for the polarization considered. Here $G(\alpha, \vec{r}) = ik/2 \int \phi_\alpha^*(x) H_0^{(1)}(k|x\vec{u}_x - \vec{r}|) dx$. Similar expressions can be obtained for the EM-fields in the reflection region and within the indentations.

III. TRANSMISSION PROPERTIES

In Ref.¹³ we analyzed, in a symmetric groove configuration, the conditions for having large transmittance, i.e. for having large E-field at the central slit. We identified three main resonant mechanisms: slit waveguide mode excitation (controlled by the metal thickness), groove cavity mode (controlled by the groove depths) and in-phase groove re-emission processes (that is maximum for wavelengths of the order of the period of the array, d). Large enhancements in the transmission for resonant wavelengths can be obtained when the three mechanisms coincide; this means that if we fix d there is an optimum value of the depth of the grooves in which the optical transmission is maximum.

In this section we present results for the total transmittance T of a system composed of a slit and, in the most general case, four periodic finite arrays of grooves. We normalize the transmittance to the incident flux in the direction normal to the metal surfaces and to the slit area. In this way T for point particles would be 1. Even with the simplifications introduced, the structure under study is still characterized by a large number of geometrical parameters. In this paper all indentation widths (a) are equal and the grooves arrays, when present, have all the same number of grooves (N). All results presented here are for $a = 40\text{nm}$, $N = 10$ and metal thickness $W = 200\text{nm}$, which are typical values considered previously in related experiments (later on we will explain the reason for choosing this particular metal thickness).

For WDM it is convenient to have at least two wavelengths transmitted primarily through the structure. Let us select, arbitrarily and simply for proof of principle purposes, $\lambda_1 = 500\text{nm}$ and $\lambda_2 = 600\text{nm}$. We consider first the even simpler system of a single slit flanked by just one groove array in the input side (IL). For the chosen values of a and N , after an optimization process of d_L and h_L we find enhanced transmission at λ_1 for $d_L = 470\text{nm}$, $h_L = 75\text{nm}$. For this set of parameters, groove cavity mode excitation and in-phase groove re-emission mechanisms are tuned to appear at λ_1 . The curve $T(\lambda)$ for this case is rendered in Fig. 2 (blue curve), showing clearly the transmission resonance at $\lambda = 500\text{nm}$ due to the presence of grooves (compare this curve with the black curve of Fig. 2, showing $T(\lambda)$ for a bare single slit). The green curve of Fig.2 presents the $T(\lambda)$ for a similar system, also with only one groove array next to the single slit but this time with lattice parameter $d_R = 560\text{nm}$ and groove depth $h_R = 95\text{nm}$ in order to have resonant transmission at $\lambda = 600\text{nm}$. Also in Fig. 2 (red curve) we show $T(\lambda)$ for the case of a single slit flanked by the two groove arrays considered previously. This last curve shows that the transmission resonances associated to each of the arrays survive, although somehow modified, the close presence of the other array. The fact that when both arrays are present the transmission peaks at $\lambda = 500$ and $\lambda = 600\text{nm}$ have the same height is neither casual nor reflects any hidden

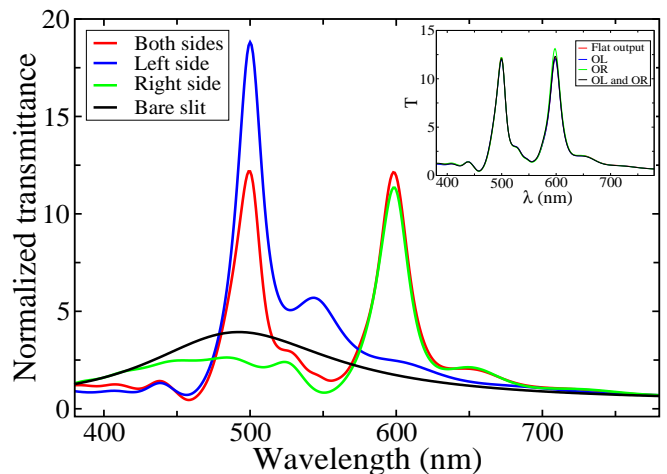


FIG. 2: Normalized-to-area transmittance plotted as a function of the wavelength for a structure defined by a flat exit surface and a input surface with grooves at both sides (red line), left side (blue line) and right side (green line). Black line corresponds to a single slit without corrugations. Inset shows the results considering grooves at both sides of the input surface and different configurations of the output surface.

property of the system: simply the value of the metal thickness ($W = 200\text{nm}$) has been tuned for this to be the case. Notice that similar transmission peak heights for the selected wavelengths is a bonus for WDM, and we just wanted to show that this condition may be fulfilled in this kind of structures. The case presented here is, however, not necessarily optimal. Probably it is possible to make the selected wavelengths to profit from slit waveguide resonances^{15,16,17,18} (the third enhancing transmission mechanism previously discussed) and get even larger transmittances. The inset to Fig. 2 shows that in asymmetric structures, as previously found for symmetric ones¹³, $T(\lambda)$ is mostly independent of the patterning of the output surface.

IV. FAR-FIELD ANGULAR DISTRIBUTION OF TRANSMITTED LIGHT

In this section we present results for the far-field angular dependence of the radial component of the Poynting vector, $S_r(\vec{r})$, evaluated in the output region. In the subwavelength limit, the transmission angular distribution of this kind of systems depends only on the output corrugation, up to a constant that accounts for the transmittance at that wavelength¹². Therefore, it is convenient to define the far-field angular transmission distribution $I(\theta) \equiv r S_r^{nor}(\theta)$ ($r \gg Nd, \lambda$), where $\vec{S}^{nor}(\lambda, \vec{r}) = \vec{S}(\lambda, \vec{r})/T(\lambda)$. Recent studies in the optical^{11,12} and microwave¹⁹ regimes have found that $I(\theta)$ for a single slit flanked by grooves arrays in the output side shows beaming effects for certain frequency ranges. In Ref.¹¹ a

phenomenological model, based on the hypothesis of the existence of a leaky wave running along the surface, was enough to explain the beaming phenomena. A subsequent first-principle model¹² supported the basics of the phenomenological approach and the origin of the leaky surface wave, and was in good agreement with the experimental data. Basically, beaming can be understood as follows: the EM field leaving the slit couples to a running surface wave (which is the result of self-consistent wandering back and forth of EM fields at the grooves, which act as surface scattering centers); this surface wave accumulates phase as it travels along the surface and it radiates to vacuum at the groove positions. So, for emission purposes, the groove array behaves as an effective diffraction grating, but illuminated at a (wavelength dependent) angle, which is related to the phase accumulated by the surface running wave. Actually, the emission intensity is different at the different radiating points of this equivalent diffraction grating, and must be calculated self-consistently from Eq.(1). However the final result shows that, at some angles, the extra optical path of waves leaving from different grooves cancel the phase of the running wave, resulting in a maximum in $I(\theta)$.

Both studies^{11,12} previously referred to considered a symmetric distribution of grooves around the central slit and, therefore, showed a symmetric $I(\theta)$. In this paper we consider asymmetric structures, showing that beaming occurs even when a slit is flanked by just a single groove array. Also we show that, to a large extent, the beam produced by a groove array is not modified if a different groove array is placed also at the output metal surface but at the other side of the slit. This is illustrated in Fig.3 where panel (a) shows $I(\lambda, \theta)$ for a system with a single groove array is placed in the OL configuration with geometrical parameters $d_L = 470\text{nm}$ and $h_L = 75\text{nm}$. Notice that, in section 3, we found that this set of parameters are optimum in order to have enhanced transmission at $\lambda_1 = 500\text{nm}$. Fig. 3a shows that this asymmetric structure presents beaming for a range of wavelengths and that maximum beaming appears at the same resonant wavelength λ_1 . It is worth noticing that even in this asymmetric case, maximum beaming occurs at $\theta = 0^\circ$. A similar representation appears in panel (b), this time for an array of grooves in OR configuration with $d_R = 560\text{nm}$ and $h_R = 95\text{nm}$ which optimizes both transmission and $I(\theta = 0^\circ)$ for $\lambda_2 = 600\text{nm}$. Panel (c) renders $I(\lambda, \theta)$ when both OL and OR arrays previously considered are present in the structure. The overall picture, more precisely lines in the $(\lambda - \theta)$ plane showing large values of $I(\lambda, \theta)$ corresponds to the addition of beaming lines of panels (a) and (b). However, panel (c) also shows that radiation coming from left and right groove arrays is not totally independent. Instead, there is a small shift in both wavelengths at which maximum beaming appears and the associated angles which now may move away from normal direction. This last fact will be of paramount importance in order to use this kind of structures as wavelength de-multiplexers.

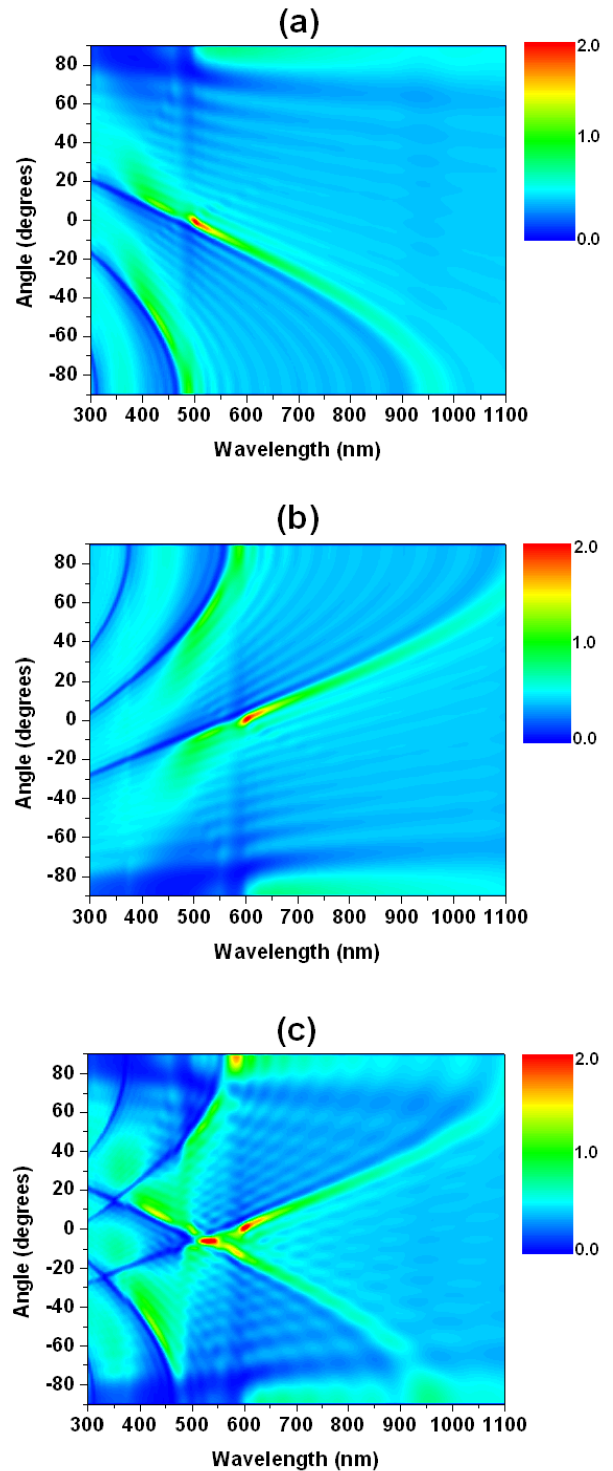


FIG. 3: Contour plots of $I(\lambda, \theta)$ with θ defined in Fig. 1. Three different configurations of the output surface are considered. (a) OL with $h=75$ nm and $d=470$ nm. (b) OR with $h=95$ nm and $d=600$ nm. (c) OL+OR with the same geometrical parameters as in (a) and (b).

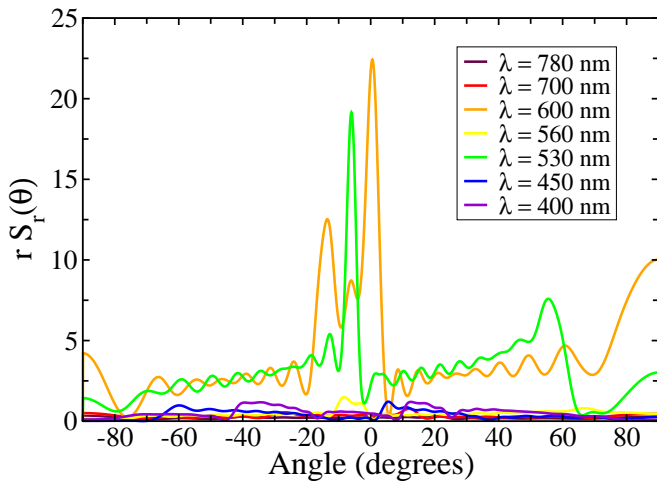


FIG. 4: Dependence of $rS_r(\theta)$ (see text) on the angle for several wavelengths. The result of each wavelength is plotted with its corresponding color in the visible spectrum. Notice beaming effect present for orange and green light.

V. WAVELENGTH DE-MULTIPLEXER DEVICE

The two abilities of these systems described in the two previous sections, namely i) the selective transmission of two wavelengths when structuring the input side of the metallic film (Section 3) and ii) beaming at the same two wavelengths in different well-defined directions (Section 4) can be combined to propose a new application of single apertures surrounded by finite arrays of grooves.: this kind of structures can be used as wavelength de-multiplexers of micro-meter dimensions. This new functionality is illustrated in Fig. 4 where $rS_r(\theta)$ in the far-field region is calculated for different wavelengths for a structure in which four groove arrays are present. Geometrical parameters of these arrays are essentially those considered in Fig.2(red curve) and Fig.3c, only that one of the grooves array in the input side has been slightly modified in order to obtain enhanced transmission at $\lambda = 530\text{nm}$. For the two resonant wavelengths ($\lambda = 530\text{nm}$ and $\lambda = 600\text{nm}$) light emerges in the form of very narrow beams presenting very low divergence (around 5°) and can be collected at an angle of 6° for $\lambda = 530\text{nm}$ and 0° for $\lambda = 600\text{nm}$. Note that due to the interplay between the left and right grooves arrays in the output side, light of wavelength 600nm can also be found at a larger collection angle of 14° . For the rest of wavelengths (see Fig.4) optical transmission is extremely low and its angular distribution is nearly uniform.

To further illustrate the resonant nature of this phenomenon, in Fig. 5 we show the near-field pictures (E-field intensity) in the output region corresponding to the transmission processes for the two resonant wavelengths ($\lambda = 530\text{nm}$ and $\lambda = 600\text{nm}$) and for a non-resonant case ($\lambda = 700\text{nm}$). For this wavelength, grooves are not playing any role; E-field intensity is low and the transmission

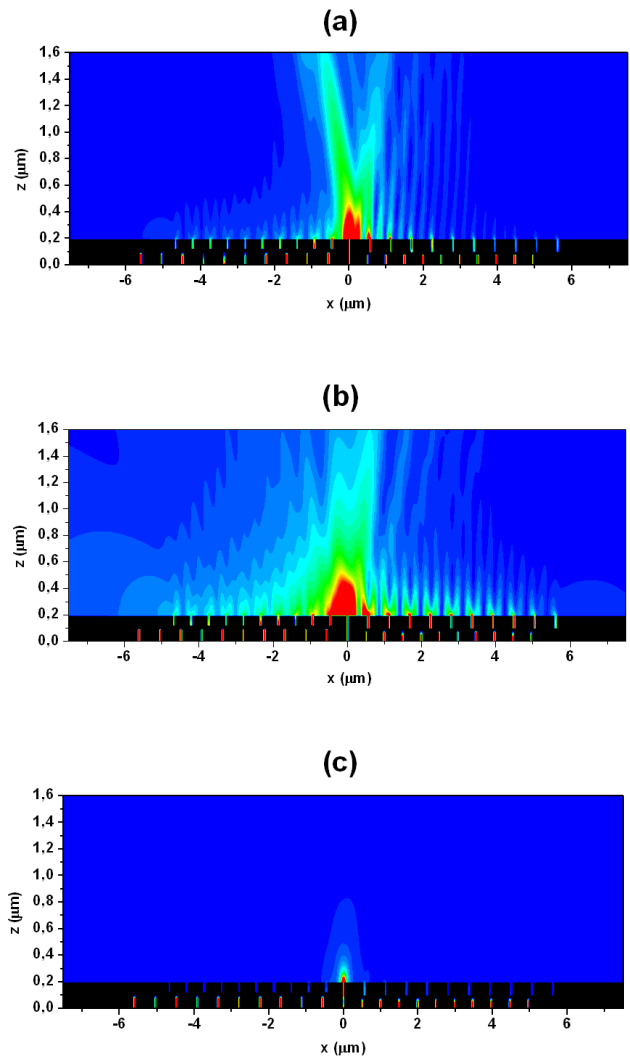


FIG. 5: Contour plots of the electric field intensity for the proposed demultiplexing structure. Three different wavelengths are considered. (a) $\lambda=530\text{ nm}$. (b) $\lambda=600\text{ nm}$. (c) $\lambda=700\text{ nm}$ (off-resonance). Red (blue) corresponds to maximum (minimum) intensity. Black areas show the metallic regions.

angular distribution is rather uniform. However in the first two cases, as clearly seen in panels (a) and (b), light is emitted not only by the central slit but also by the grooves located at left and right sides of the aperture in the output side. As a result of the interference between these re-emission processes narrow beams of light emerge from the structure and are already present in the near-field regime. Fingerprints of the running surface waves that are at the origin of the beaming phenomena can also be visualized in these pictures.

In conclusion, we have shown how a single subwavelength aperture surrounded by finite arrays of indentations may be used as a wavelength de-multiplexer. The

two selected wavelengths can be chosen by just modifying the geometrical parameters defining the structure (period of the arrays at left and right of the central slit and widths and depths of the indentations). A practical advantage of this type of *plasmon* wavelength demultiplexer device with respect to others based on, for example, photonic crystals²⁰ is that light emerging from our proposed device forms two collimated beams presenting both a very low divergence. This divergence can also be controlled and reduced by increasing the number of indentations in the output side. Implementation of this device to build up a multi-frequency de-multiplexer can be achieved by just adding up other single apertures and the corresponding indentations with the appropriate geometrical parameters to the structure analyzed in this

communication. The fact that input and output corrugations seem to act independently and also that the interplay between left and right indentations is weak allows us to state that this type of structured metals could be used as building-blocks of several opto-electronic devices of reduced dimensions.

Acknowledgements

Financial support by the Spanish MCyT under grant BES-2003-0374 and contracts MAT2002-01534 and MAT2002-00139 is gratefully acknowledged.

-
- ¹ M.M. Sigalas, C.T. Chan, K.M. Ho and C.M. Soukoulis, Phys. Rev. B, **52**, 11744 (1995).
² W. L. Barnes, T.W. Preist, S.C. Kitson, and J.R. Sambles, Phys. Rev. B **54**, 6227 (1996).
³ F. J. Garcia-Vidal and J. B. Pendry, Phys. Rev. Lett. **77**, 1163 (1996).
⁴ S. Fan, P. R. Villeneuve, and J. D. Joannopoulos, Phys. Rev. B, **54**, 11245 (1996).
⁵ D. F. Sievenpiper, E. Yablonovitch, J.N. Winn, S. Fan, P.R. Villeneuve, and J.D. Joannopoulos, Phys. Rev. Lett. **80**, 2829 (1998).
⁶ J. B. Pendry, Science **285**, 1687 (1999).
⁷ J.G. Fleming, S.Y. Lin, I.El-Kady, R. Biswas, and K.M. Ho, Nature (London) **417**, 52 (2002).
⁸ T. W. Ebbesen, H.J. Lezec, H.F. Ghaemi, T. Thio, and P.A. Wolff, Nature (London) **391**, 667 (1998).
⁹ D. E. Grupp, H.J. Lezec, T. Thio, and T.W. Ebbesen, Adv. Mater. **11**, 860 (1999).
¹⁰ T. Thio, K.M. Pellerin, R.A. Linke, H.J. Lezec, and T.W. Ebbesen, Opt. Lett. **26**, 1972 (2001).
¹¹ H.J. Lezec, A. Degiron, E. Devaux, R.A. Linke, L. Martín-Moreno, F.J. Garcia-Vidal, and T.W. Ebbesen, Science **297**, 820 (2002).
¹² L. Martín-Moreno, F.J. García-Vidal, H.J. Lezec, A. Degiron, and T.W. Ebbesen, Phys. Rev. Lett. **90**, 167401 (2003).
¹³ F.J. García-Vidal, H.J. Lezec, T.W. Ebbesen, and L. Martín-Moreno, Phys. Rev. Lett. **90**, 213901 (2003).
¹⁴ F.J. García-Vidal and L. Martín-Moreno, Phys. Rev. B **66**, 155412 (2002).
¹⁵ J. A. Porto, F. J. García-Vidal, and J. B. Pendry, Phys. Rev. Lett. **83**, 2845 (1999).
¹⁶ S. Collin, F. Pardo, R. Teissier, and J.-L. Pelouard, Phys. Rev. B **63**, 033107 (2001).
¹⁷ Y. Takakura, Phys. Rev. Lett. **86**, 5601 (2001).
¹⁸ F. Yang and J.R. Sambles, Phys. Rev. Lett. **89**, 063901 (2002).
¹⁹ A.P. Hibbins, J.R. Sambles, and C.R. Lawrence, Appl. Phys. Lett. **81**, 4661 (2002).
²⁰ S. Noda, A. Chutinan, and M. Imada, Nature **407**, 608 (2000); H. Kosaka *et al.*, Phys. Rev. B **58**, R10096 (1998); T. Baba and M. Nakamura, IEEE Journal of Quantum Electronics, **38**, 909 (2002).